Electric Power Systems Research 218 (2023) 109218

Contents lists available at ScienceDirect

Electric Power Systems Research

journal homepage: www.elsevier.com/locate/epsr

MMC-based topology for grid connection of wind generators with phase and arm power balancing

Fernando Martinez-Rodrigo [a,*], Santiago de Pablo [a], Dionisio Ramirez [b], Luis C. Herrero-De Lucas [a], Zaid A. Aljawary [a,c]

[a] Departamento de Tecnologia Electronica, Universidad de Valladolid, Valladolid 47011, Spain
[b] Centre of Industrial Electronics (CEI), Universidad Politécnica de Madrid (UPM), Madrid 28006, Spain
[c] Department of Biomedical Engineering, Qaiwan International University-UTM franchise, Sulaimaniyah, KRG, Iraq

ARTICLE INFO

Keywords:
Modular Multilevel Converter (MMC)
Multilevel converter
Wind energy conversion
Wind energy integration
Wind farms
Wind power grid integration

ABSTRACT

A new topology of a wind farm wherein the wind generators are integrated into the structure of a modular multilevel converter (MMC) is presented. It allows connecting a group of small/medium size wind turbines to the grid, replacing all the grid side converters of the wind generators by the MMC. The different power generated by each wind generator causes power imbalances that can lead to circulating currents; this paper addresses this problem by analyzing it in a simple way. The analysis shows that power differences between phases are naturally balanced by the DC component of circulating current, without the need to use a specific regulator. However, the power differences between the arms result in a high 50 Hz circulating current. This paper presents the design of a new regulator that corrects these power imbalances by generating a phase difference between the upper and lower arm voltages resulting in an optimal 50 Hz circulating current. The operation of the MMC-based wind farm topology has been tested when all the turbines generate the same power and when they generate significantly different powers. Numerical and real-time simulation results show that the proposed regulator keeps the powers of the MMC phases and arms balanced.

1. Introduction

Wind generators (WG) are controlled using a machine-side converter (MSC) and a grid-side converter (GSC) connected to the grid employing a step-up transformer [1]. The MSC controls electromagnetic torque and magnetic field in the electric generator and is in charge of tracking the maximum power point (MPPT) of the wind turbine [2,3], whereas the GSC is in charge of keeping the DC link voltage constant and controlling the reactive power injected into the grid. A drawback of this configuration is that uses twice as many power converters as wind turbines.

This paper proposes a new wind farm topology wherein the grid connection is designed to take advantage of the MMC topology to reduce the number of power converters. In effect, the integration of the wind generators into the MMC structure makes the use of GSCs unnecessary.

The MMC topology was initially developed for power transmission using high-voltage direct current (HVDC) in long-distance point-to-point applications [4–6]. Some examples are the connection of islands or wind farms to the grid [7]. Other applications are related to medium voltage such as STATCOM [8,9], and low voltage such as the control of WG [10].

The integration of PV and/or battery storage (BS) in the structure of MMCs has already been analyzed by some authors since it presents some advantages over conventional structures, mainly in medium voltage. Next, the state of the art of this topic, which is the most directly related to this article, is explained.

Energy storage in batteries connected to medium voltage power grids is and will continue to be a relevant topic in the future. Conventional two or three-level converters use a large number of batteries connected in series, which presents reliability problems and has led to the possibility of including that storage in the modules of an MMC in order to use batteries of lower rated voltage [11–13]. One advantage of this configuration is by using non-isolated DC/DC converters in the connection of the batteries to the switching module (SM) capacitors, so it makes possible to remove the low-frequency components from the output current of the SMs. Moreover, the control loops allow a state of charge (SOC) balancing in the phases and arms, and operation under unbalanced grid voltages [12]. However, this configuration also has

* Corresponding author.
E-mail address: fernando.martinez@uva.es (F. Martinez-Rodrigo).

https://doi.org/10.1016/j.epsr.2023.109218
Received 13 September 2022; Received in revised form 19 December 2022; Accepted 10 February 2023
Available online 16 February 2023

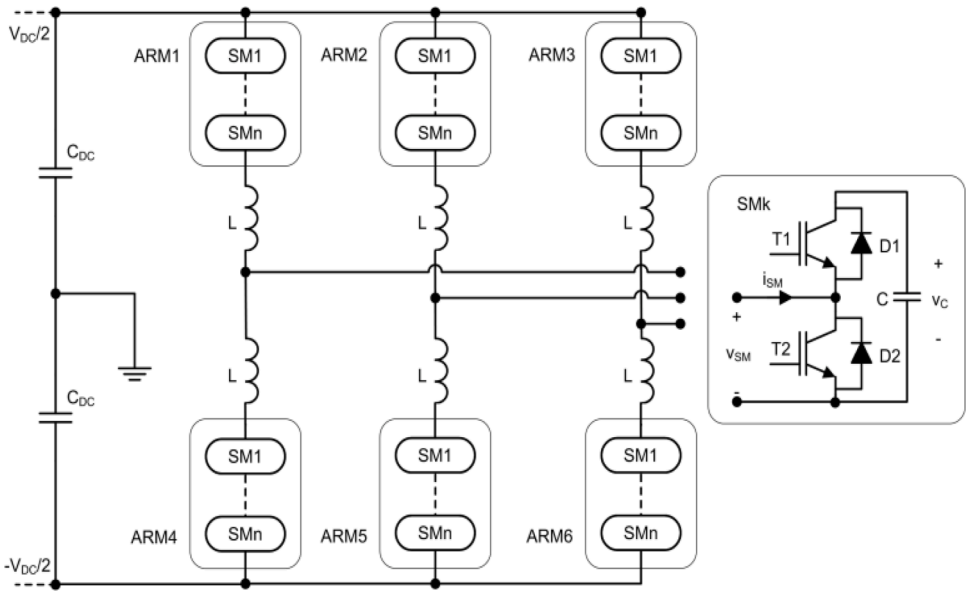

Fig. 1. Standard modular multilevel converter (MMC); includes SMs with HB topology.

disadvantages since, when a part of the SMs do not include storage, the algorithms that are usually used to balance the voltage of the capacitors cause a reduction of the available PQ regions [11].

In [13], an MMC with distributed BS in its SMs, a cascade converter with distributed BS in its H-bridge (two legs with two transistors each) SMs, and an MMC with centralized BS in its DC link are compared and the analysis showed that the first one provides the most efficient, reliable and versatile solution.

Another application of BS integration into the MMC structure is presented in [14]. In this case, it is used to integrate a fleet of electric vehicles (EV) into the grid; an energy management strategy using an SOC model and the coordinated control of the energy flow between the arms of the same and different phases is proposed.

Some approaches integrate a group of solar panels into the structure of an MMC [15,16]. The connection to the SM through an isolated DC/DC converter allows the MPPT of each group of panels individually and the elimination of the grid connection transformer. Furthermore, the power of the phases can be balanced using a DC differential current, and the DC voltages of the SMs can be balanced using an AC differential current [15]. Using this approach, a multi-megawatt PV plant can be connected to the grid via an MMC using full-bridge SMs, with MPPT capability, higher power quality, higher efficiency, fault tolerance, smaller filter size, and lower transformer voltage ratio [16].

Some authors have proposed combining solar panels and batteries and incorporating them into the structure of the MMC to smooth the variations in PV generation caused by variations in solar radiation. In this case, some SMs incorporate solar panels and other SMs have batteries, all connected through insulated DC/DC converters. To avoid each phase delivering a different power to the grid, the differences in power generation between phases and arms are compensated by exchanging power between the arms [17].

Other authors propose strategies to compensate for the reduction in the power generated by the panels due to transient shading. In [18] it is proposed to include a solar panel in each SM of an MMC and to control the voltage of each SM to carry out the MPPT of each solar panel. This avoids using a DC/DC converter on each SM. Furthermore, it is proposed to add a redundant module in each arm to keep the DC voltage of each arm constant.

In [19], the advantages provided by the integration of decentralized energy resources (DER) in the SMs of the MMC were analyzed, resulting in the need to transfer energy between arms and between phases to balance them. Consequently, the authors develop a methodology based on the equations that control the power transmission between arms to keep the modules' voltage balanced. In that way, it is also possible to reduce the second and third harmonics that appear when the DERs are present only in some of the SMs.

Unlike the papers presented to date, this paper proposes the integration of a group of small/medium size wind generators into the structure of an MMC, so that each SM includes a WG but removes its GSC, which largely reduces the number of necessary semiconductors. In a conventional structure, each wind turbine employs 12 IGBTs distributed across the MSC and the GSC. In the proposed structure, based on using a single MMC, each wind turbine requires one MSC and one SM cell, that is, 8 IGBTs, which represents 4 IGBTs less for each wind turbine.

Although several authors have studied how to balance the powers between phases and between arms using regulators so that each grid phase receives the same power, this paper presents an original and different approach that is easier to interpret, both in terms of theoretical analysis and the use of regulators. In this paper, power balancing between phases is achieved in a natural way through the DC component of the circulating current, and without the need to use a specific regulator, unlike other papers in which regulators are used for this task.

Power balancing between arms is achieved by means of a regulator whose input is the difference between the voltages of the upper and lower arms capacitors, and whose output is a phase shift between the voltages of the two arms that causes an optimal circulating current at the fundamental frequency. This regulator is a new and simpler contribution than those proposed in the technical literature.

In addition, simulations and experimental results show that, despite the imbalances in power generation between phases and between arms, the power transfer to the grid is balanced.

The paper is structured as follows. Section 2 presents the new wind farm topology integrated into an MMC, the control loops for the DC voltage and the grid connection, the PWM generator, and the voltage sorting algorithm. In Section 3, the theoretical analysis of the power transfer between phases and between arms is carried out. Then, the solutions to keep the power delivery to the grid by each phase and the SM voltages balanced are proposed. Section 4 is devoted to the design of the new controller to balance the powers generated in the upper and lower arms. Section 5 shows the simulation results for three cases: (i) balanced generation, (ii) unbalanced phase generation, and (iii) unbalanced arm generation; in the final part of this section, the simulation results are analyzed to assess the operation of the proposed solution.

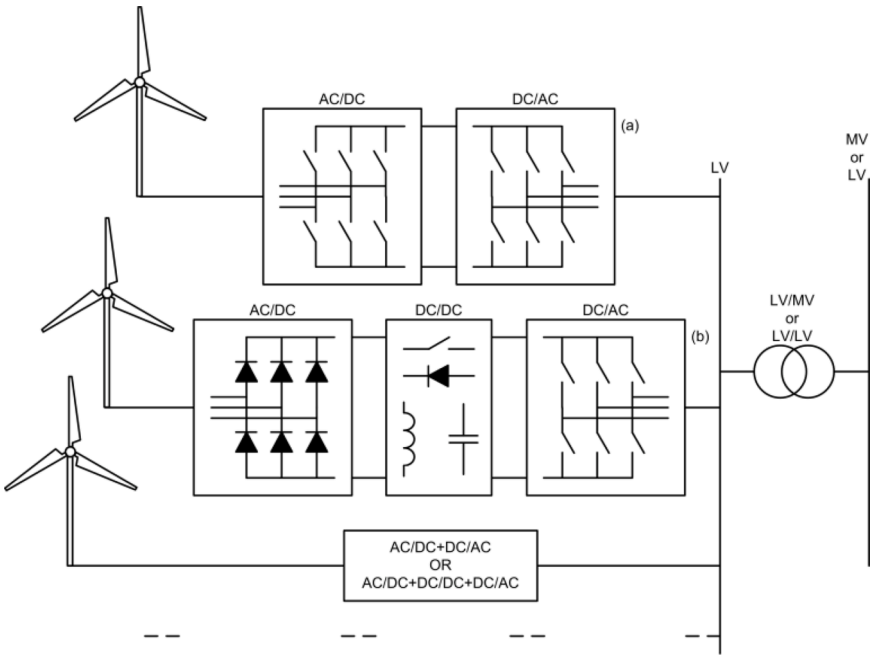

Fig. 2. Typical configuration for the grid connection of small turbines. Converters may include: (a) AC/DC + DC/AC, or, (b) diode rectifier + DC/DC + DC/AC (only in very small turbines).

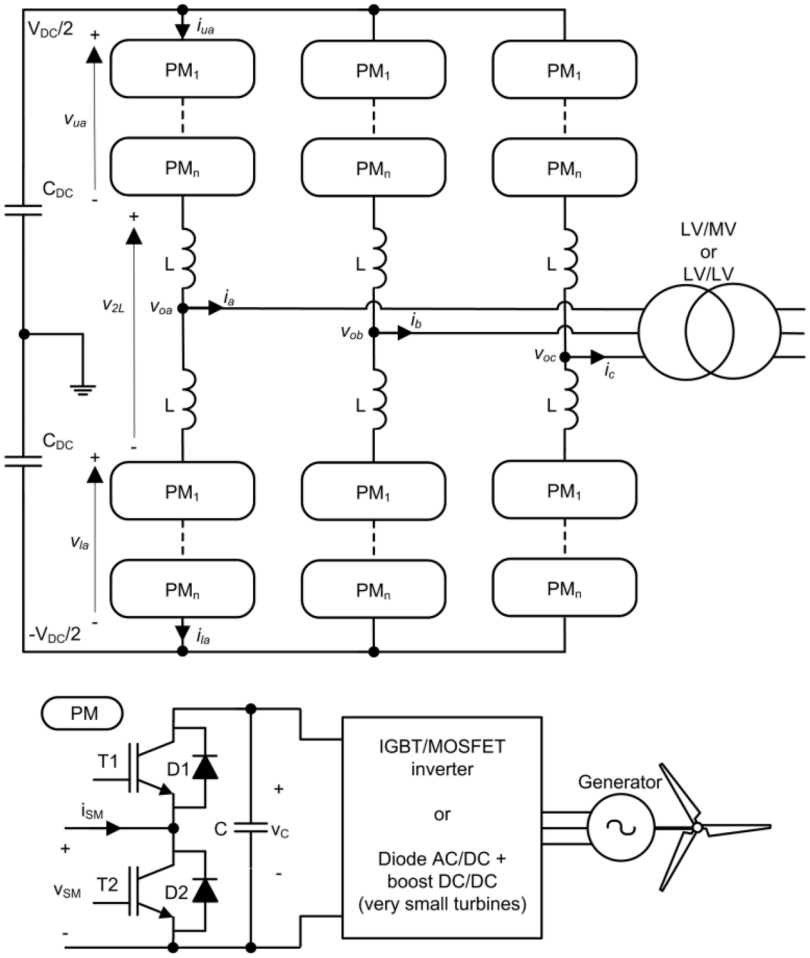

Fig. 3. Top: connection of the PMs into the MMC. Below: integration of the WGs into the PMs.

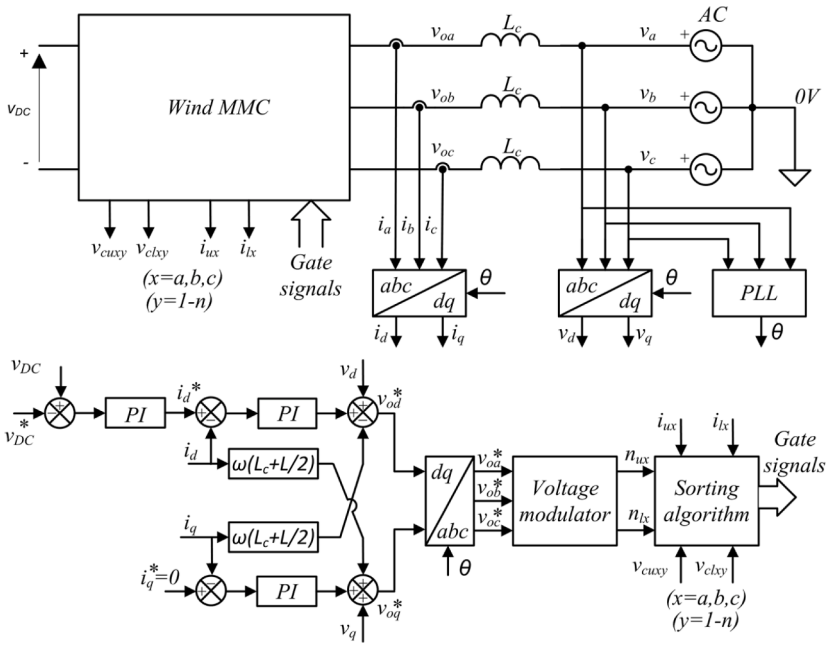

Fig. 4. Block diagram used in the control of the MMC grid connection.

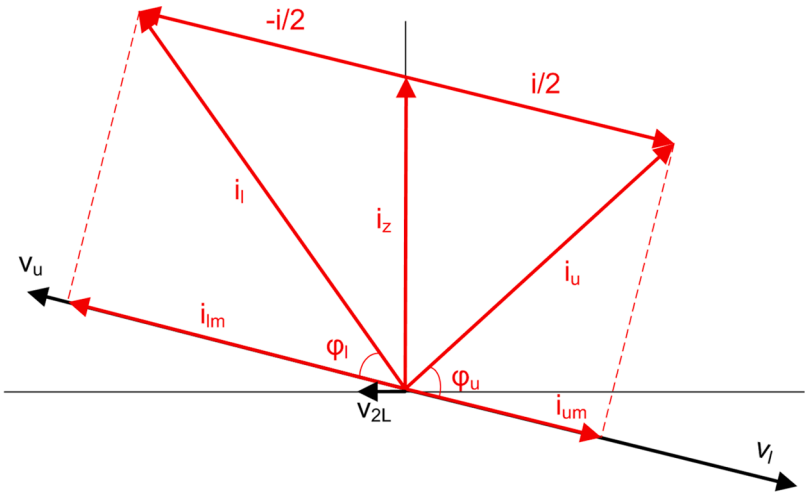

Fig. 5. Voltage and current phasors at 50 Hz when the circulating current is not on the same line as the arm currents.

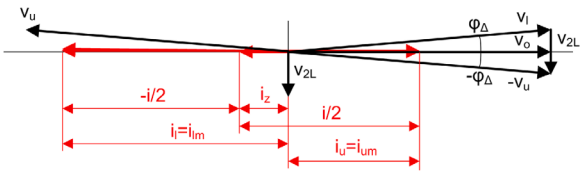

Fig. 6. Voltage and current phasors at 50 Hz when the circulating current is on the same line as the arm currents.

Section 6 shows the experimental results obtained through real-time simulation. Finally, Section 7 presents the conclusions of this work.

2. Connection structure and control system

A standard MMC (Fig. 1) comprises three phases, an upper and a lower arms per phase, and *n* SM per arm. The electric power can be transferred between the alternating current (AC) side and the direct current (DC) side of the converter, and a certain amount of reactive power can be injected into the AC grid. The MMC shown in Fig. 1 is built using SMs, in an half-bridge (HB) setup, which includes two IGBTs, two diodes, and one capacitor. A detailed explanation of the SM operation and the voltage-current relationships can be found in [20].

The usual configuration of small wind turbines connected to the grid (Fig. 2) comprises two DC/AC converters for each turbine, or, in very small turbines, a diode rectifier, a DC/DC converter (booster), and one inverter. The inverters are connected in parallel to the input of a step-up transformer, whose output can be either low voltage (LV) or medium voltage (MV), depending on the number and size of the wind turbines.

The proposed new topology is intended to reduce the high number of semiconductors involved in the abovementioned configurations. To this end, the WGs are proposed to be integrated into the structure of an MMC (Fig. 3). The SMs of the MMC are now named power modules (PM) in the new drive, and they include a wind turbine, a permanent magnet synchronous generator (PMSG), and an inverter or, in very small turbines, one diode rectifier plus one DC/DC boost converter [21,22]. In the new topology, the GSC of the WG is replaced by the HB of the corresponding

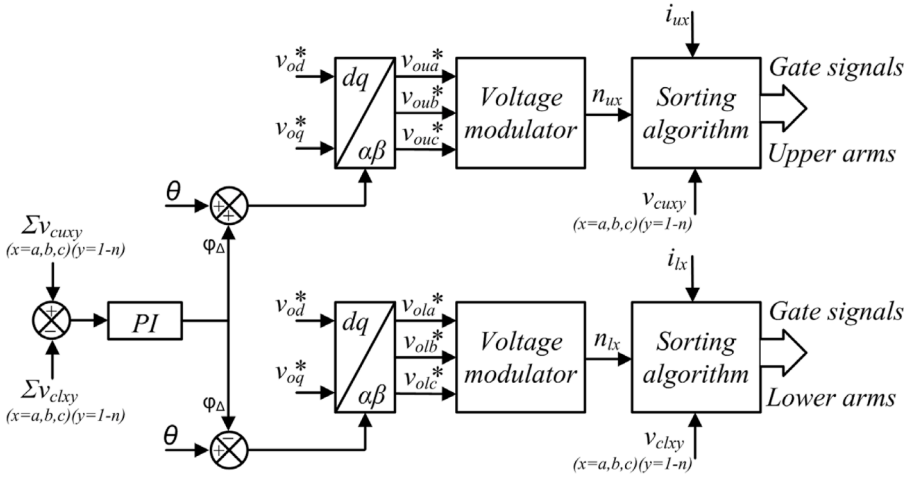

Fig. 7. Controller for balancing the voltages of the upper and lower arm capacitors.

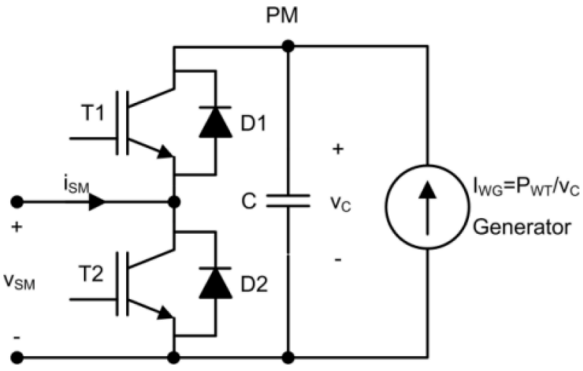

Fig. 8. PM simulation model.

Table 1
Simulation parameters.

n	5	i_q^*	0
T_S	1 μs	$k_{p,VDC}$	3.2
T_{PWM}	250 μs	$k_{i,VDC}$	64
T_{reg}	125 μs	$k_{p,id,iq}$	0.5
v_{DC}	2.4 kV	$k_{i,id,iq}$	5
C	600 mF	$k_{p,PLL}$	0.2
L	937.5 μH	$k_{i,PLL}$	2
$v_{ph,ph}$	1300 V_{RMS}	$k_{p,\Sigma Vc}$	0.00001
L_c	750 μH	$k_{i,\Sigma Vc}$	0.0001
C_{DC}	200 μF		

SM, thus reducing from 6 to 2 the number of IGBTs per WG. That represents the first contribution of this paper.

In a conventional MMC (Fig. 1), the power is exchanged between the DC side and the AC side of the converter. However, in the proposed topology (Fig. 3), no incoming DC power exists since the power generated by the wind generators is delivered directly to the grid as AC. The power generated in each upper/lower arm, $p_{WTu(l)x}$, with $x = a,b,c$, is the addition of the power generated by each turbine in the upper/lower arm $p_{WTu(l)xy}$, with $y = 1,\ldots,n$:

$$p_{WTu(l)x} = \sum_{y=1}^{n} p_{WTu(l)xy} \quad (1)$$

Fig. 4 shows the block diagram used in the grid connection control of the MMC. The voltage and current control loops use a reference frame where the d axis is aligned with space vector corresponding to the grid voltage v_{abc}, whose frequency, ω, and angle, θ, are detected by the phase-locked loop (PLL). The DC voltage, v_{DC}, is regulated by a PI controller whose output is the current reference in the direct axis, i_d^*. The q axis current reference equals zero, $i_q^* = 0$, to set the reactive power exchanged with the grid to zero. The output voltage references, v_{od}^* and v_{oq}^*, are obtained using two PI controllers and the corresponding decoupling terms.

The voltage reference of each phase of the converter, v_{oabc}^*, is the input to a voltage modulator, which implements phase disposition-sinusoidal pulse width modulation (PD-SPWM) [23], and whose output is the number of PMs in the ON state of the upper/lower arm, $n_{u(l)x}$. Other modulators that can be used are multi-level PWM [24], multi-level space vector modulation (SVM) [25] and nearest level control (NLC) [26], or even current modulators [27]. When the number of levels is low it is better to use PWM or SVM rather than NLC to eliminate low frequency harmonics. To reduce the harmonic content and place it in multiples of the carrier frequency it is better to use PWM than current modulation. PD-SPWM has been chosen over SVM because of its greater simplicity.

The last control block is the PM sorting algorithm, [24,28], which is in charge of balancing the voltage of the capacitors of each arm, so that $v_C = v_{DC}/n$, using the values of the capacitor voltages and the direction of the arm current; its output is the trigger signal of each PM. However, other sorting methods can also be used [29,30].

Keeping constant the DC link voltage, v_{DC}, is of paramount importance and means that the entire power generated by the turbines must be delivered to the grid. Otherwise, the difference between the power generated by the turbines and the power delivered to the grid will be stored or extracted from the capacitors, and the voltage v_{DC} will increase or decrease, respectively.

The voltages and currents in the converter have three frequencies (three harmonics): continuous component, 50 Hz (fundamental component), and 100 Hz (2nd harmonic), assuming a 50 Hz utility grid. The continuous component of the circulating current balances the differences of the power generated in each phase, sending power from the phases that generate more power to those that generate less.

The 50 Hz components are responsible for transferring power from the turbines to the grid. Notice that the power delivered by each phase of the MMC to the grid is the same, $p_a = p_b = p_c = p_x$, since this is assured by its vector control.

The 100 Hz components are circulating currents present in any MMC and are extensively discussed in the literature [31,32]. In this paper, the variables represent 50 Hz voltages and currents; when they refer to other components, DC or 100 Hz, it is specifically stated.

Only balanced and non-distorted electrical grids have been considered, but specific control strategies for unbalanced [20] or distorted grids [33] can be used.

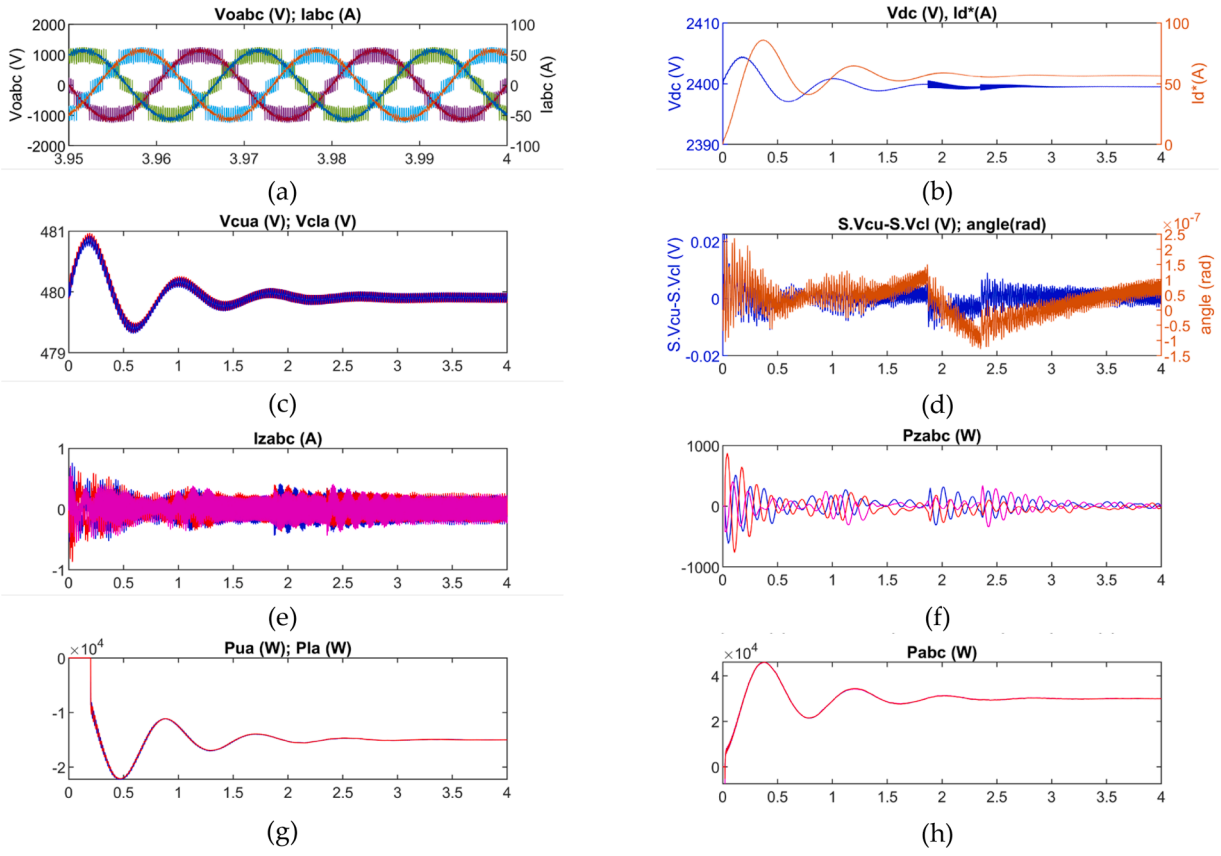

Fig. 9. Simulation graphs when all the modules of phases a, b and c generate a power of 3 kW: (a) output voltages and output currents, (b) DC voltage and current i_d^*, (c) voltages of the capacitors of the upper and lower arm SMs of the first phase (voltages are superimposed), (d) input and output of the regulator to balance the voltages of the upper and lower arm capacitors, (e) circulating currents, (f) power transferred between phases, (g) power generated by the upper and lower arms of the first phase, and (h) active power delivered by each phase. Time in seconds.

3. Wind power generation - case studies

Three cases regarding the power generated by the WGs have been studied: (a) all the WGs generate the same power, (b) all the WGs of a phase generate the same power, which is different from the power generated by the WGs of the other phases, (c) all the phases generate the same total power, but the powers generated by the upper and lower arms are different.

3.1. All the WGs generate the same power

Since all the WGs generate the same power, p_{1WT}, the upper and lower arms of all the phases produce the same power, $p_{WTua} = p_{WTla} = p_{WTub} = p_{WTlb} = p_{WTuc} = p_{WTlc} = np_{1WT}$. The power generated in phase x $(x = a, b, c)$, $p_{WTux} + p_{WTlx} = 2np_{1WT}$, is sent to the corresponding AC output, $p_{WTux} + p_{WTlx} = p_x$.

Therefore, in this case no additional control is needed to achieve a balanced distribution of power in the phases.

3.2. The WGs generate a power that depends on the phase to which they are connected

In this case, the power generated by the WGs of the upper and lower arms of each phase is the same, but different from the power generated in other phases, $p_{WTua} = p_{WTla} \neq p_{WTub} = p_{WTlb} \neq p_{WTuc} = p_{WTlc}$. Since the power to be delivered by the MMC in AC through each phase is the same, a DC power transfer must take place from the phases that generate more power to those that generate less power.

The circulating current of each phase i_{Zx} consists of a DC component and an AC component,

$$i_{Zx} = i_{ZDCx} + i_{ZACx} \tag{2}$$

The DC power that phase x sends to the other two phases, p_{Zx}, is the product of the average value of its circulating current, i_{ZDCx}, and the DC voltage, v_{DC},

$$p_{Zx} = -i_{ZDCx} \cdot v_{DC} \tag{3}$$

Since the sum of the continuous components of the circulating currents is zero,

$$i_{ZDCa} + i_{ZDCb} + i_{ZDCc} = 0 \tag{4}$$

the sum of the DC powers transferred between phases is zero as well,

$$p_{Za} + p_{Zb} + p_{Zc} = 0 \tag{5}$$

The difference between the power generated in the upper and lower arms of the phase, $p_{WTux} + p_{WTlx}$, and the power delivered to the grid by the phase, p_x, is equal to the power that this phase transfers to the others,

$$p_{Zx} = (p_{WTux} + p_{WTlx}) - p_x \tag{6}$$

Therefore, the average value of the circulating currents is responsible for the power transfer between phases.

In other publications for PV sources, where the MMC is connected to a stiff DC source, the sum of the three circulating currents is not zero, so a regulator is used to balance the power generated in the three phases. In this work, this regulator is not necessary since no DC source is included and the virtual voltage of the DC link is kept constant by means of an external regulation loop; this is the second contribution of this paper.

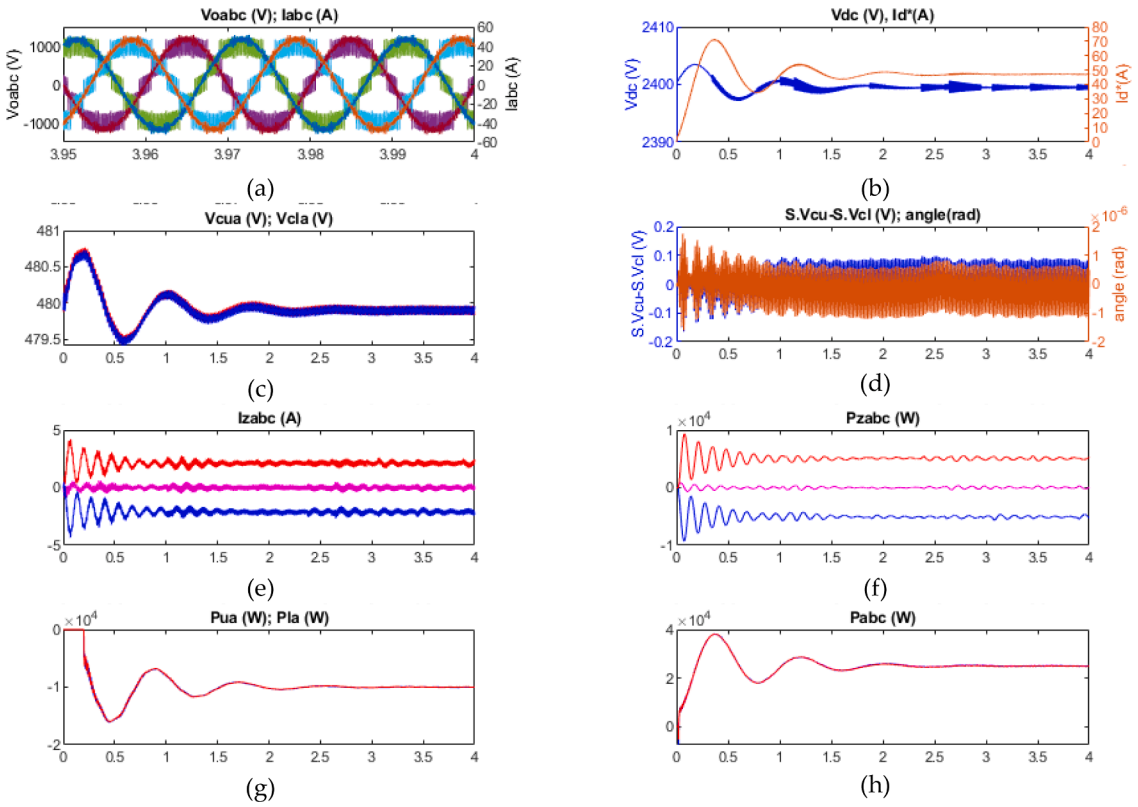

Fig. 10. Simulation graphs when all modules of phases a, b and c generate a power of 2 kW, 2.5 kW, and 3 kW, respectively: (a) output voltages and output currents, (b) DC voltage and current $i_d{}^*$, (c) voltages of the capacitors of the upper and lower arm SMs of the first phase (voltages are superimposed), (d) input and output of the regulator to balance the voltages of the upper and lower arm capacitors, (e) circulating currents, (f) power transferred between phases, (g) power generated by the upper and lower arms of the first phase, and (h) active power delivered by each phase. Time in seconds.

3.3. Each phase generates the same power, but the powers generated by the upper and lower arms are different

The conditions considered in this case are: (a) the powers generated by the WGs of the upper arms are equal in the three phases, $p_{WTua} = p_{WTub} = p_{WTuc} = p_{WTu}$, (b) the powers generated by the WGs of the lower arms are equal, $p_{WTla} = p_{WTlb} = p_{WTlc} = p_{WTl}$, and (c) the powers generated by the WGs of the upper and lower arms are different, $p_{WTu} \neq p_{WTl}$.

From this paragraph onwards, subscript *x*, meaning a generic phase, will be removed for the sake of simplicity; it should be understood that all the variables correspond to a phase *x*.

In a standard MMC, the current of the upper/lower arm is [28,34]:

$$i_{u(l)} = \pm\frac{i}{2} + \frac{i_{DC}}{3} + i_Z \tag{7}$$

In the proposed MMC structure there is nothing connected to the DC side, so the current of the DC side is zero, $i_{DC} = 0$,

$$i_{u(l)} = \pm\frac{i}{2} + i_Z \tag{8}$$

The circulating AC currents present two main harmonics, the 1st and 2nd which, in countries with a grid frequency of 50 Hz, correspond to 50 Hz and 100 Hz, respectively. The 2nd harmonic, i_{ZAC2}, is very common in the circulating currents of any MMC [31,32]. The harmonic 1, i_{ZAC1}, is the quotient between the voltage of the two inductances of the same phase, v_{2L1}, (Fig. 3), and the impedance of the two inductances of a phase, $2Z_{L1}$, all at the frequency of the first harmonic (50 Hz).

$$i_{ZAC1} = \frac{v_{2L1}}{2Z_{L1}} \tag{9}$$

At the frequency of harmonic 1, the sum of the voltages of the upper arm v_{uAC}, the lower arm v_{lAC} and the two inductances is zero (sub-index 1 is removed for simplicity; when it is referred to other harmonic, it will be noted):

$$v_{uAC} + v_{2L} + v_{lAC} = 0 \rightarrow v_{2L} = -(v_{uAC} + v_{lAC}) \tag{10}$$

The voltage of the upper/lower arm, neglecting the voltage of the arm's inductances, is:

$$v_{u(l)} = \frac{\sum v_{C_{u(l)}}}{2} + v_{u(l)AC} \tag{11}$$

where $\sum v_{C_{u(l)}}$ is the sum of the voltages of the *n* capacitors of the upper/lower arm. When the voltages of the capacitors of the upper and lower arms are equal, $\sum v_{C_u} = \sum v_{C_l} = v_{DC}$, the AC components of the arms are equal,

$$v_{u(l)AC} = \mp v_o \tag{12}$$

and the voltage of the arms is:

$$v_{u(l)} = \frac{v_{DC}}{2} \mp v_o \tag{13}$$

The instantaneous power delivered by the upper/lower arm is:

$$p_{u(l)} = -v_{u(l)} \cdot i_{u(l)} = -\left(\frac{\sum v_{C_{u(l)}}}{2} + v_{u(l)AC}\right) i_{u(l)} \tag{14}$$

And the average power delivered by each upper/lower arm results in

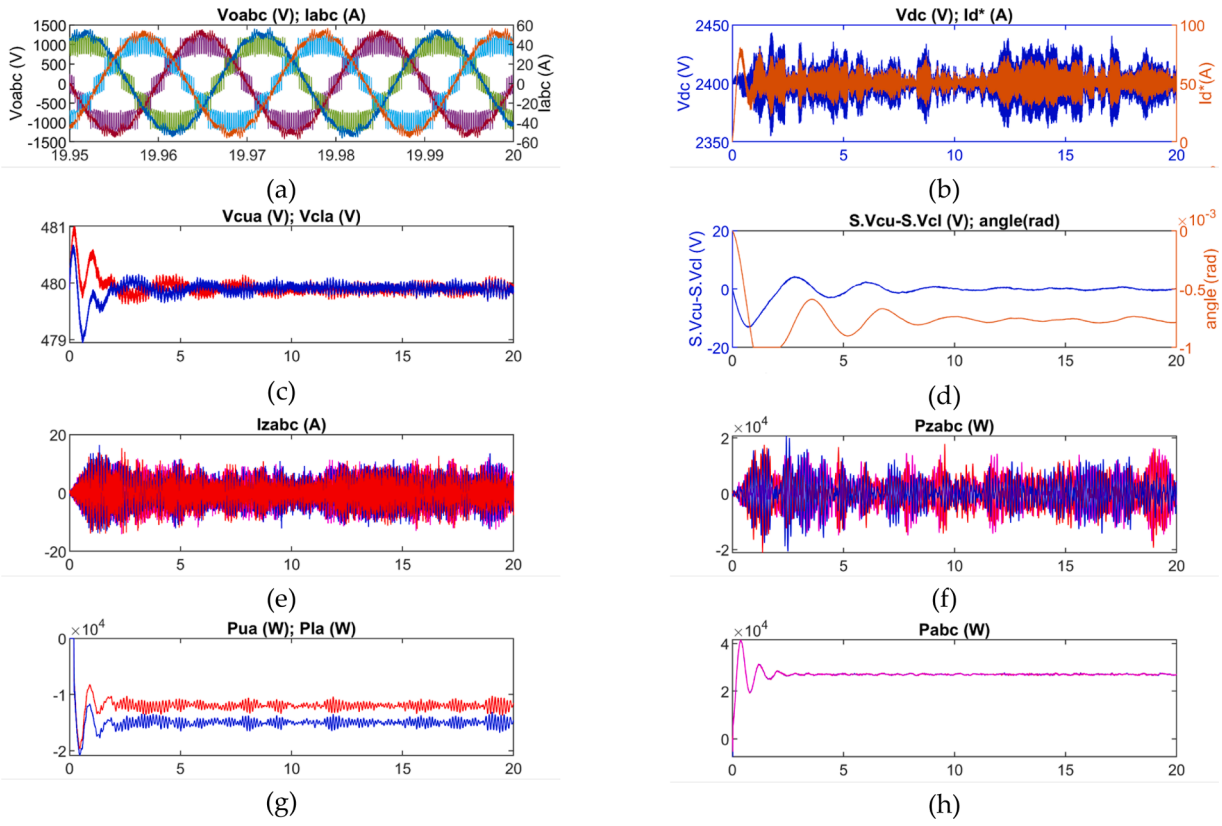

Fig. 11. Simulation graphics when two upper modules, in each phase, generate 1.5 kW, and the rest generate 3 kW: (a) output voltages and output currents, (b) DC voltage and current $i_d{}^*$, (c) voltages of the capacitors of the upper and lower arm SMs of the first phase (voltages are superimposed), (d) input and output of the regulator to balance the voltages of the upper and lower arm capacitors, (e) circulating currents, (f) power transferred between phases, (g) power generated by the upper and lower arms of the first phase, and (h) active power delivered by each phase. Time in seconds.

$$P_{u(l)} = \frac{1}{T}\int_0^T p_{u(l)}(t)dt = \frac{1}{T}\int_0^T -\left(\frac{\sum v_{C_{u(l)}}}{2} + v_{u(l)AC}\right) i_{u(l)}dt$$
$$= 0 + \frac{1}{T}\int_0^T -v_{u(l)AC} i_{u(l)}dt \tag{15}$$

where $\int_0^T -\frac{\sum v_{C_{u(l)}}}{2} i_{u(l)}dt = 0$ because the current of the upper/lower arm, $i_{u(l)}$, is sinusoidal and the voltage $\frac{\sum v_{C_{u(l)}}}{2}$ is constant. Therefore, the power delivered by the upper/lower arm is calculated by the fundamental component (50 Hz) of the voltage $v_{u(l)AC}$ and the current $i_{u(l)}$ of the arm.

Assuming that initially the voltages of all the capacitors were equal, and using the Eqs. (9), (10) and (12), the circulating current would be zero, and the current of the arms, according to (8), has the same value but opposite polarity,

$$i_{u(l)} = \pm\frac{i}{2} \tag{16}$$

In this case, the power delivered by the upper and lower arms, obtained by means of (12), (15) and (16), results in

$$P_{u(l)} = \frac{1}{T}\int_0^T -v_{u(l)AC} i_{u(l)}dt = \frac{1}{T}\int_0^T -(\mp v_o)\left(\pm\frac{i}{2}\right)dt = \frac{1}{T}\int_0^T v_o\frac{i}{2}dt \tag{17}$$

However, since the power generated by the turbines of the upper and lower arms is different, $p_{WTu} \neq p_{WTl}$, the energy of the capacitors of the arm $W_{\sum C_{u(l)}}$ increases or decreases,

$$\frac{dW_{\sum C_{u(l)}}}{dt} = p_{WTu(l)} - p_{u(l)} \tag{18}$$

The capacitors of the arm that generates higher power will be charged and those of the arm that generates lower power will be discharged. That causes the reduction of the AC voltage of the arm whose capacitors are being discharged and the increase of the AC voltage of the arm whose capacitors are being charged, keeping the modulation index of each one:

$$m = \frac{\widehat{v}_o}{v_{DC}/2} \tag{19}$$

$$m_{u(l)} = \frac{\widehat{v}_{u(l)AC}}{\sum v_{C_{u(l)}}/2} \tag{20}$$

$$m_{u(l)} = m \tag{21}$$

According to (20), the variation of the capacitor voltages causes the arm peak voltages, $\widehat{v}_{u(l)AC}$, to be different, which, according to (10), causes a voltage of 50 Hz to be present in the arm inductances v_{2L}. According to (9), that generates a circulating current of 50 Hz, i_{ZAC1}, which, according to (8), causes the current of each arm, $i_{u(l)}$, to be different. Thus, according to (17), the power delivered by each arm is different. Finally, an equilibrium point is reached in which each arm delivers the same power as it generates, and in which the capacitor voltages stabilize.

This situation is illustrated in Fig. 5, where it can be seen how the circulating current, i_Z, is delayed by 90° with respect to the voltage v_{2L}. Although v_{2L} has a low value, the current i_Z may have a high value due to the low value of the inductance 2L. As shown in Fig. 5, the power

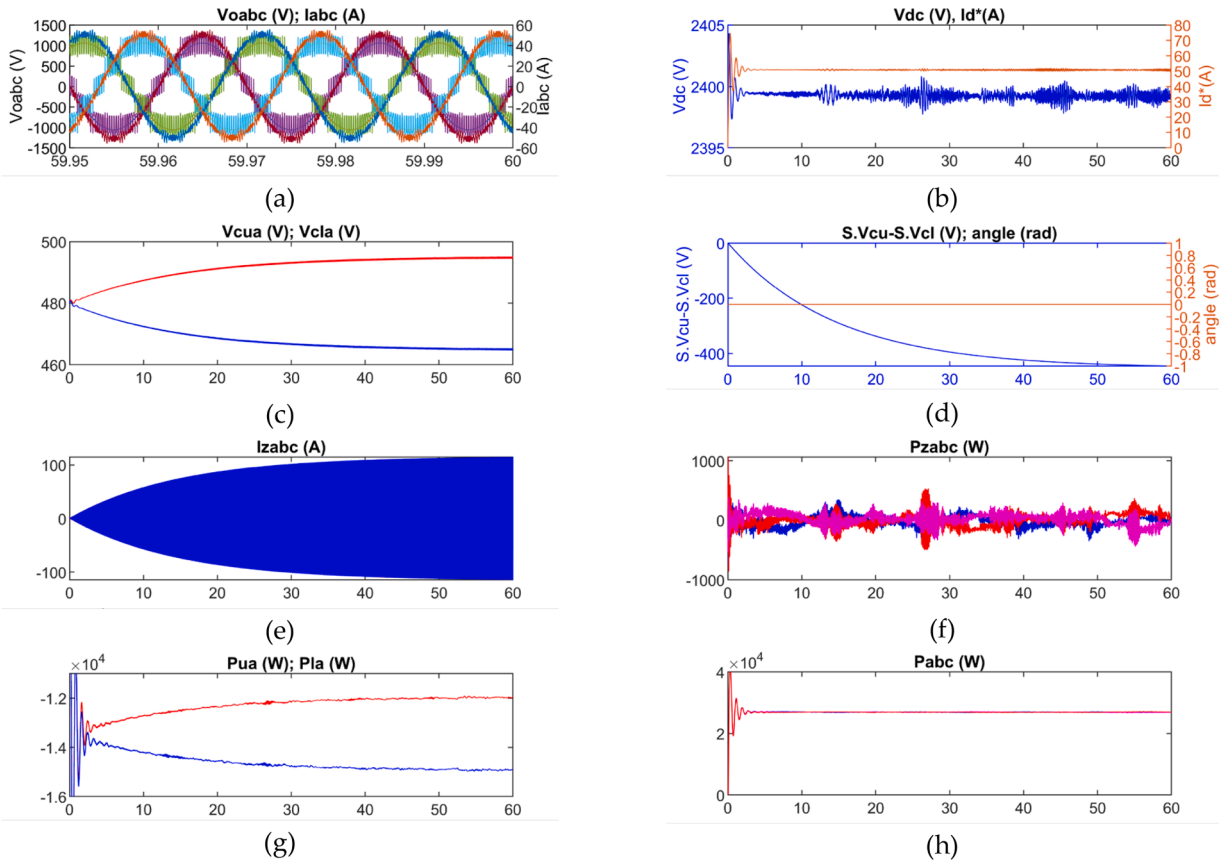

Fig. 12. Simulation graphs when no controller is used to balance the voltage of the upper and lower capacitors; two upper modules, in each phase, generate 1.5 kW, and the rest generate 3 kW: (a) output voltages and output currents, (b) DC voltage and current i_d^*, (c) voltages of the capacitors of the upper and lower arm SMs of the first phase (voltages are superimposed), (d) input and output of the regulator to balance the voltages of the upper and lower arm capacitors, (e) circulating currents, (f) power transferred between phases, (g) power generated by the upper and lower arms of the first phase, and (h) active power delivered by each phase. Time in seconds.

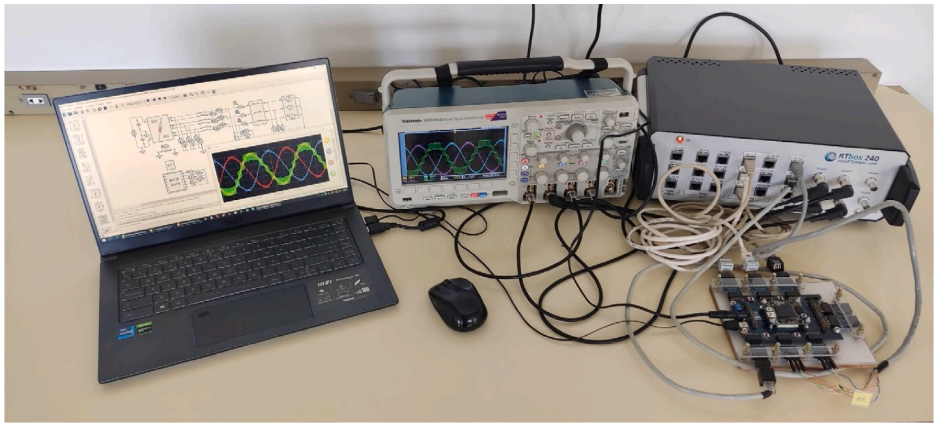

Fig. 13. Photograph of the tests with the RTS.

delivered by each arm can be calculated as:

$$P_{u(l)} = v_{u(l)rms} i_{u(l)rms} \cos\varphi_{u(l)} = v_{u(l)rms} i_{u(l)mrms} \tag{22}$$

Fig. 5 shows a situation where the control of the voltages of the upper and lower arms is not independent and the power generated in the lower arm is greater than that generated in the upper arm. As a consequence of this imbalance, the voltage of the lower capacitors, $\sum v_{C_l}$, is slightly higher than that of the upper ones, $\sum v_{C_u}$, and the voltage of the lower arm, v_l, is slightly higher than that of the upper arm, v_u; the magnitude of these voltages is very similar and also very similar to the value of the output voltage, v_o. Under these conditions, i_{um} is smaller than i_{lm} so that the power delivered by the upper arm, P_u, is lower than that delivered by the lower arm, P_l.

This is not the ideal situation since the value of the upper/lower arm current $i_{u(l)}$ is greater than the optimum, $i_{u(l)m}$; in Section 4 a solution to solve this issue is proposed.

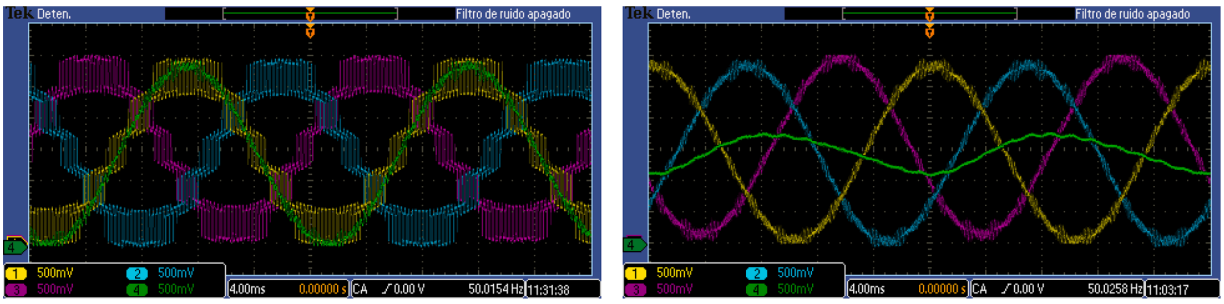

(a) (b)

Fig. 14. RTS graphs when all the modules of phases a, b and c generate a power of 3 kW (case 1): (a) output voltages (400 V/div), and (b) output currents (20 A/div) and circulating current of the first phase (2 A/div). Time scale: 4 ms/div.

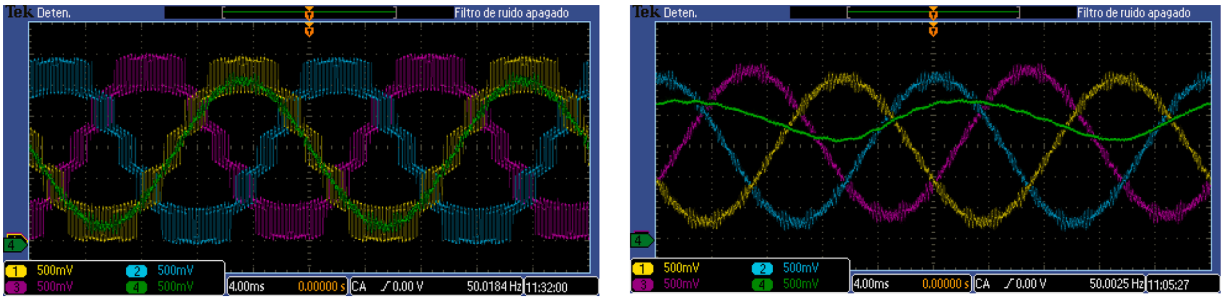

(a) (b)

Fig. 15. RTS graphs when all modules of phases a, b and c generate a power of 2 kW, 2.5 kW, and 3 kW, respectively (case 2): (a) output voltages (400 V/div), and (b) output currents (20 A/div) and circulating current of the first phase (2 A/div). Time scale: 4 ms/div.

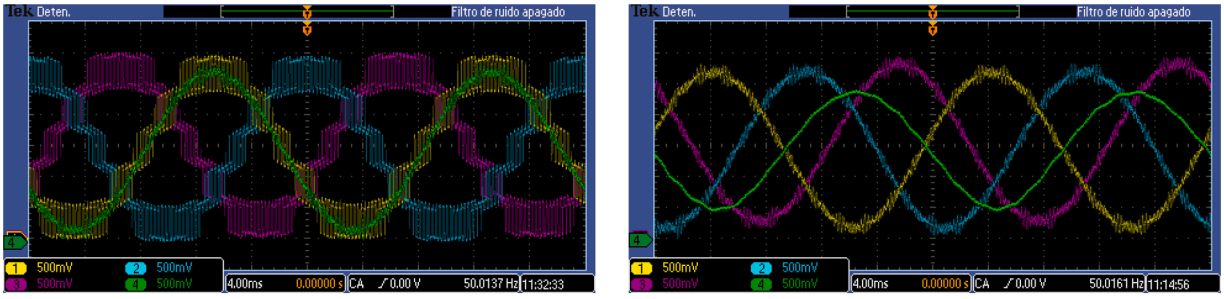

(a) (b)

Fig. 16. RTS graphics when two upper modules, in each phase, generate 1.5 kW, and the rest generate 3 kW (case 3): (a) output voltages (400 V/div) and output current of the first phase (20 A/div), and (b) output currents (20 A/div) and circulating current of the first phase (2 A/div). Time scale: 4 ms/div.

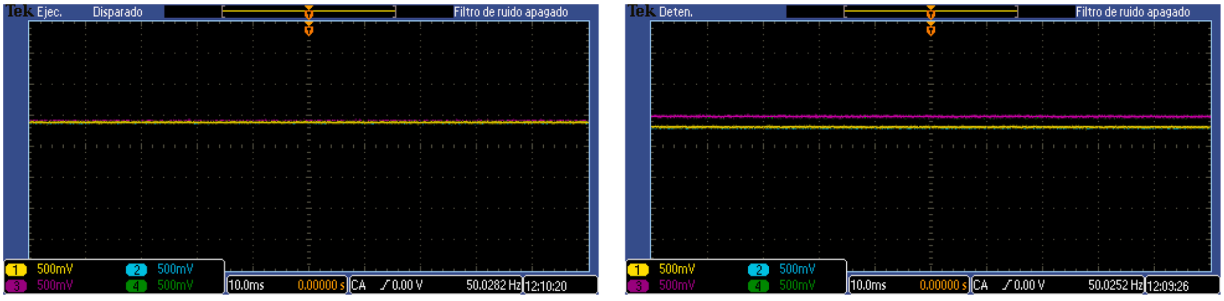

(a) (b)

Fig. 17. RTS graphics when two upper modules, in each phase, generate 1.5 kW, and the rest generate 3 kW (case 3). Voltage of two upper and two lower arm capacitors (100 V/div): (a) with regulator (the four graphs are superimposed), and (b) without regulator (the graphs are superimposed by two and two). Time scale: 10 ms/div.

4. Design of a PI controller for balancing the power generated in the upper and lower arms

When the power generated in the upper and lower arms is different, a situation of non-optimal balance is reached, as indicated in Section 3.3, where the circulating current is not aligned with the arm voltages $v_{u(l)}$ (Fig. 5).

Fig. 6 shows the ideal situation, where the arm currents, $i_{u(l)}$, have the minimum possible value, being approximately aligned with the arm voltage, $v_{u(l)}$ (note: the angles represented in Fig. 6, φ_Δ, are actually extremely small but in the figure have been enlarged to improve the visualization). From the converter output voltage, v_o, the voltages of both arms can be calculated by adding and subtracting an angle φ_Δ, so that the phases of the arm inductance voltage, v_{2L}, and the circulating current, i_z, are 270° and 180°, respectively.

In view of that, a PI controller that takes care of balancing the capacitor voltages of the upper and the lower arms of the three phases has been developed, which constitutes the third contribution of this paper. Its input is the difference between the addition of voltages of the capacitors in the upper arms of the three phases, $\sum_{\substack{x=a,b,c\\y=1,\dots,n}} v_{C_{uxy}}$, and the addition of voltages of the capacitors in the lower arms of the three phases, $\sum_{\substack{x=a,b,c\\y=1,\dots,n}} v_{C_{lxy}}$, (Fig. 7). Its output is the angle φ_Δ that must be added or subtracted to the reference voltage $v_o{}^*$ to obtain the references $v_{ou}{}^*$ or $v_{ol}{}^*$, respectively.

Compared to previous works, the analysis of the power unbalance in the arms presented in this paper is simpler and the proposed work-around minimizes the circulating current at the fundamental frequency.

5. Simulation results

The simulation results have been obtained using Matlab/Simulink software, which has been selected because it has detailed models of the components that allow a very detailed and reliable simulation, besides being a very common software in the simulation of power electronic converters.

Each PM is simulated using a current source (Fig. 8), which represents the power of a wind turbine, and includes the generator and the converter shown in Fig. 3. In an actual application, the converter is responsible for controlling the rotation speed of the turbine through the electromagnetic torque in order to generate the maximum electrical power.

The rated power and DC voltage of the wind turbines represented in the simulation are 3 kW and 240 Vdc, respectively, and correspond to the small wind turbine Wind 25.2+ of the manufacturer Bornay. The rest of the simulation parameters are gathered in Table 1.

5.1. All the turbines generate the same power

When all the WGs generate the same power, 3 kW, all arms and all phases produce the same power and there is no need to transfer power between phases or arms. The voltage regulator is responsible for maintaining the balance between the power generated and the power delivered to the grid.

The graphs obtained in the simulations are shown in Fig. 9. Fig. 9a shows the sinusoidal waveforms of both, output voltages, v_{oabc}, and output currents, i_{abc}. The DC voltage, v_{DC}, features an initial transient because the initial value of the current $i_d{}^*$ is zero (Fig. 9b).

In the graphs of $v_{C_{ua}}$ and $v_{C_{la}}$, the voltages of all PM capacitors of the upper and lower arms of phase *a* overlap (Fig. 9c). As can be seen, all PMs have the same voltage, not needing to activate the balancing controller of the upper and lower arms (the angle has a negligible value) since the upper and lower arms generate the same power (Fig. 9d).

Fig. 9e shows the small value of the circulating currents, i_{zabc}. The DC power transferred between phases, P_{zabc}, is zero because the generated power is the same in the three phases (Fig. 9f). The power generated by the upper and lower arms is equal (15 kW) (Fig. 9g). The active power delivered by each phase, P_{abc}, has the same shape as $i_d{}^*$ (Fig. 9h). Summarizing, the whole system works correctly.

5.2. The power generated by the wind turbines depends on the phase to which they are connected

In this section, an unbalance in the power generated by the wind turbines of the three phases has been simulated. Specifically, each wind turbine of phases a, b and c generate 2 kW, 2.5 kW, and 3 kW, respectively. As each phase comprises 10 PMs phases a, b and c generate 20 kW, 25 kW, and 30 kW, respectively. As all the phases inject the same AC power, P_{abc}, into the grid, each one injects 25 kW (Fig. 10h), which is the average value of the three phases. For this, phase c transfers 5 kW to phase a.

Fig. 10a shows the output voltage of the three phases and the low ripple sinusoidal output currents. The DC voltage, v_{DC}, evolves towards the reference value after a transient caused by $i_d{}^*(0) = 0$ (Fig. 10b).

The voltages of the capacitors of the upper, v_{Cua}, and lower, v_{Cla}, arms of the first phase are equal (Fig. 10c). The output of the controller developed to balance the voltages of the upper and lower capacitors is very low (Fig. 10d), because it does not have to act when the upper and lower arms generate the same power (Fig. 10g).

The circulating currents, i_{zabc}, feature a low ripple, and a non-zero average value in phases a and c which allows transferring power from phase c to phase a (Fig. 10e). In the graph of transferred DC power between phases, P_{zabc}, can be seen that phase a receives 5 kW and phase c delivers 5 kW, while phase b does not exchange DC power (Fig. 10f).

5.3. Each phase generates the same power, but the powers generated by the upper and lower arms are different

In this case, phases a, b and c generate the same power, but there is an unbalance between the power generated in the upper and lower arms. In the upper arms, three PMs generate 3 kW and two PMs generate 1.5 kW, and therefore each upper arm generates a total of 12 kW. In the lower arms, the five PMs generate 3 kW, with a total of 15 kW.

As explained in Section 3.3, when no action is taken to transfer different power from the upper and lower arms to the grid, the voltages of the upper and lower arm capacitors decrease and increase, respectively, until a situation of equilibrium is reached in which the AC component of the upper and lower arm voltages is reduced and increased, respectively. This causes an increase of the voltage in the inductances of the arms, v_{2L}, and, as a consequence, of the circulating current, i_z. In turn, this causes the variation of the current of the upper arm, i_u, and lower arm, i_l, to balance the power generated and delivered by the arm (see Fig. 5).

When the voltages of the upper and lower arms are controlled independently, the circulating current can be controlled to make them take the minimum value necessary to achieve the balance of the powers (Figs. 6 and 7), so that the difference between capacitors' voltages is much smaller (Fig. 11d). In this figure can be seen how the controller that controls the difference between the voltages of the upper and lower arms, modifies the phase shift of the upper and lower arm voltages in a value of approximately $-7,5{\cdot}10^{-4}$ radians to achieve that the upper and lower capacitor voltages are equal.

As can be seen in Fig. 11, the rest of the variables perform well.

The case in which the regulator in Fig. 7 has not been included has been simulated (Fig. 12). Initially, all the capacitors have a voltage of $v_{C_{ua}} = v_{C_{la}} = 480\ V$ (Fig. 12c); the power delivered by each arm is the same, $P_{ua} = P_{la} = 13.5\ kW$ (Fig. 12g), and therefore the capacitor voltages change, the upper capacitors are discharged and the lower ones are charged, until reaching $v_{C_{ua}} = 465\ V$ and $v_{C_{la}} = 495\ V$ after $t = 60\ s$ (Fig. 12c). Then, an equilibrium point is reached in which each arm

generates the same power as it delivers, $P_{ua} = 12\ kW$ and $P_{la} = 15\ kW$ (Fig. 12g). However, this equilibrium point is worse than when a regulator is used (Fig. 11) because the circulating currents are much higher (Fig. 12e).

6. Experimental results

To obtain the experimental results, the RTbox 240 real-time simulator (RTS) from accuRTpower.com was used for the plant and an FPGA board from Trenz Electronic was used for the controller (Fig. 13), in which the same schemes simulated in Section 5 (Figs. 4, 7 and 8) and the same simulation parameters (Table 1) were included. Results have been obtained for the same three cases: balanced generation, phase unbalanced generation and arm unbalanced generation.

6.1. All the turbines generate the same power

When each module generates the same power of 3 kW (case 1), the output voltages and output currents generated by Simulink (Fig. 9a) are the same as those obtained by the RTS (Fig. 14). The circulating current has a very small value in both cases (Figs. 9e and 14b).

6.2. The power generated by the wind turbines depends on the phase to which they are connected

When the powers generated in each SM of phases a, b and c are, respectively, 2 kW, 2.5 kW and 3 kW (case 2), the output voltages and currents obtained through Simulink (Fig. 10a) and through the RTS (Fig. 15) are the same. The circulating current presents a similar average value (Figs. 10c and 15b), corresponding to the power transfer between phases a and c, as well as a very low ripple.

6.3. Each phase generates the same power, but the powers generated by the upper and lower arms are different

Case 3 is analyzed below, when the power generated by each of the upper and lower arms is 12 kW and 15 kW, respectively. Fig. 16 shows the results obtained using the RTS when the proposed regulator is used to balance the voltages of the upper and lower capacitors; it can be seen that the output voltages and currents have similar values (Figs. 11a and 16) and that the circulating currents remain at moderate and similar values (Figs. 11e and 16b). Fig. 17 shows the module capacitor voltages; when the regulator is used (Figs. 11c and 17a), the capacitor voltages of the upper and lower arms maintain the same value, while when the regulator is not used, these voltages take different voltages (Figs. 12c and 17b).

7. Conclusions

A new way of connecting small wind turbines to the electrical grid has been presented. This first contribution makes it possible to reduce the number of power converters needed to integrate the WGs into the structure itself of an MMC.

The control system for the new structure consists of two loops. The outer loop keeps the DC voltage constant by delivering all incoming power from the WGs to the grid. In addition, that loop controls the reactive power injected into the grid.

The second contribution is the inner loop. This loop keeps the voltage of the MMC modules balanced so that it can be connected to the grid using PWM. The difficulties caused by power generation unbalances between phases and between arms have been analyzed, and it has been concluded that unbalances between phases can be solved, without needing a specific controller, through the average value of the circulating currents. This property avoids using a specific controller for that purpose, as was usual until now in other works.

The third contribution is the design of a controller that removes unbalances between the upper and lower arms, avoiding the circulating currents becoming too high.

Although the paper is particularized for wind generators, the structure of the connection is also valid for other generators such as PV panels or wave energy converters.

CRediT authorship contribution statement

Fernando Martinez-Rodrigo: Conceptualization, Methodology, Software, Validation, Investigation, Writing – original draft. **Santiago de Pablo:** Conceptualization, Methodology, Software, Validation, Investigation, Resources. **Dionisio Ramirez:** Conceptualization, Methodology, Investigation, Writing – original draft. **Luis C. Herrero-De Lucas:** Validation, Formal analysis, Data curation, Writing – review & editing, Supervision. **Zaid A. Aljawary:** Formal analysis, Data curation, Writing – review & editing, Supervision.

Declaration of Competing Interest

The authors declare that they have no known competing financial interests or personal relationships that could have appeared to influence the work reported in this paper.

Data availability

The data that has been used is confidential.

References

[1] R. Engleitner, A. Nied, M.S.M. Cavalca, J.P. Da Costa, Dynamic analysis of small wind turbines frequency support capability in a low-power wind-diesel microgrid, IEEE Trans. Ind. Appl. (2018), https://doi.org/10.1109/TIA.2017.2761833.
[2] K. Yenduri, P. Sensarma, Maximum power point tracking of variable speed wind turbines with flexible shaft, IEEE Trans. Sustain. Energy. (2016), https://doi.org/10.1109/TSTE.2015.2510422.
[3] A.A.A. Radwan, Y.A.I. Mohamed, Grid-connected wind-solar cogeneration using back-to-back voltage-source converters, IEEE Trans. Sustain. Energy. 11 (2020) 315–325, https://doi.org/10.1109/TSTE.2019.2890828.
[4] M. Davies, M. Dommaschk, J. Dorn, J. Lang, D. Retzmann, D. Soerangr, HVDC PLUS – Basics and Principle of Operation, Siemens Ag, 2011, pp. 1–24.
[5] C. Mahimkar, N. Persson, G. Westerlind, HVDC Technology for Large Scale Offshore Wind Connections, Smartelec, Vadodara, India, 2013, pp. 1–5.
[6] HVDC-VSC, Transmission Technology of the Future, Alstom Grid, 2011, pp. 13–17. http://www.tresamigasllc.com/docs/ThinkGrid08-06-Chapter1-Art1VSC_EN.pdf.
[7] A. Abdalrahman, E. Isabegovic, DolWin1 - Challenges of connecting offshore wind farms, in: 2016 IEEE Int. Energy Conf. ENERGYCON 2016, 2016, https://doi.org/10.1109/ENERGYCON.2016.7513981.
[8] S. Du, J. Liu, A study on dc voltage control for chopper-cell-based modular multilevel converters in D-statcom application, IEEE Trans. Power Deliv. (2013), https://doi.org/10.1109/TPWRD.2013.2246195.
[9] H.P. Mohammadi, M.T. Bina, A transformerless medium-voltage STATCOM topology based on extended modular multilevel converters, IEEE Trans. Power Electron. (2011), https://doi.org/10.1109/TPEL.2010.2085088.
[10] Y. Gangui, L. Jigang, M. Gang, L. Yu, L. Yang, S. Wei, Research on modular multilevel converter suitable for direct-drive wind power system, Energy Procedia 17 (2012) 1497–1506, https://doi.org/10.1016/j.egypro.2012.02.272.
[11] T. Soong, P.W. Lehn, Assessment of fault tolerance in modular multilevel converters with integrated energy storage, IEEE Trans. Power Electron. (2016), https://doi.org/10.1109/TPEL.2015.2477834.
[12] M. Vasiladiotis, A. Rufer, Analysis and control of modular multilevel converters with integrated battery energy storage, IEEE Trans. Power Electron. (2015), https://doi.org/10.1109/TPEL.2014.2303297.
[13] T. Soong, P.W. Lehn, Evaluation of emerging modular multilevel converters for BESS applications, IEEE Trans. Power Deliv. (2014), https://doi.org/10.1109/TPWRD.2014.2341181.
[14] M. Mao, Y. Ding, L. Chang, N.D. Hatziargyriou, Q. Chen, T. Tao, Y. Li, Multi-objective power management for EV fleet with MMC-based integration into smart grid, IEEE Trans. Smart Grid. (2019), https://doi.org/10.1109/TSG.2017.2766363.
[15] H. Bayat, A. Yazdani, A power mismatch elimination strategy for an MMC-based photovoltaic system, IEEE Trans. Energy Convers. (2018), https://doi.org/10.1109/TEC.2018.2819982.
[16] S. Rivera, B. Wu, R. Lizana, S. Kouro, M. Perez, J. Rodriguez, Modular multilevel converter for large-scale multistring photovoltaic energy conversion system, in: 2013 IEEE Energy Convers. Congr, Expo. ECCE, 2013, p. 2013, https://doi.org/10.1109/ECCE.2013.6646945.

[17] A.Y.H. Bayat, A hybrid MMC-based photovoltaic and battery energy storage system, IEEE Power Energy Technol. Syst. J. 6 (2019) 32–40, https://doi.org/10.1109/JPETS.2019.2892418.
[18] F. Rong, X. Gong, S. Huang, A novel grid-connected PV system based on MMC to get the maximum power under partial shading conditions, IEEE Trans. Power Electron. (2017), https://doi.org/10.1109/TPEL.2016.2594078.
[19] T. Soong, P.W. Lehn, Internal power flow of a modular multilevel converter with distributed energy resources, IEEE J. Emerg. Sel. Top. Power Electron. (2014), https://doi.org/10.1109/JESTPE.2014.2342656.
[20] D. Ramirez, F. Martinez-Rodrigo, S. de Pablo, L. Carlos Herrero-de Lucas, Assessment of a non linear current control technique applied to MMC-HVDC during grid disturbances, Renew. Energy. 101 (2017) 945–963, https://doi.org/10.1016/j.renene.2016.09.050.
[21] J.M. Guerrero, C. Lumbreras, D. Reigosa, D. Fernandez, F. Briz, C.B. Charro, Accurate rotor speed estimation for low-power wind turbines, IEEE Trans. Power Electron. 35 (2020) 373–381, https://doi.org/10.1109/TPEL.2019.2913781.
[22] A. Chub, O. Husev, A. Blinov, D. Vinnikov, Novel isolated power conditioning unit for micro wind turbine applications, IEEE Trans. Ind. Electron. (2017), https://doi.org/10.1109/TIE.2016.2645890.
[23] V.G. Agelidis, M. Calais, Application specific harmonic performance evaluation of multicarrier PWM techniques, in: PESC Rec, IEEE Annu. Power Electron. Spec. Conf. (1998) 172–178, https://doi.org/10.1109/PESC.1998.701896.
[24] S. Rohner, S. Bernet, M. Hiller, R. Sommer, Modulation, losses, and semiconductor requirements of modular multilevel converters, IEEE Trans. Ind. Electron. 57 (2010) 2633–2642, https://doi.org/10.1109/TIE.2009.2031187.
[25] S. De Pablo, A.B. Rey-Boué, L.C. Herrero, F. Martínez, Hexagon based algorithm for space vector modulation on multilevel voltage source inverters, in: IEEE Int. Symp. Ind. Electron., 2010, pp. 3218–3223, https://doi.org/10.1109/ISIE.2010.5637592.
[26] F. Martinez-Rodrigo, L.C. Herrero-de Lucas, S. de Pablo, A.B. Rey-Boué, D. Ramirez, Calculation of the number of modules and the switching frequency of a modular multilevel converter using near level control, Electr. Power Syst. Res. (2018), https://doi.org/10.1016/j.epsr.2018.08.019.
[27] F. Martinez-Rodrigo, S. de Pablo, L.C. Herrero-de Lucas, Current control of a modular multilevel converter for HVDC applications, Renew. Energy. 83 (2015) 318–331, https://doi.org/10.1016/j.renene.2015.04.037.
[28] M. Saeedifard, R. Iravani, Dynamic performance of a modular multilevel back-to-back HVDC system, IEEE Trans. Power Deliv. 25 (2010) 2903–2912, https://doi.org/10.1109/TPWRD.2010.2050787.
[29] M. Hagiwara, H. Akagi, Control and experiment of pulsewidth-modulated modular multilevel converters, IEEE Trans. Power Electron. (2009), https://doi.org/10.1109/TPEL.2009.2014236.
[30] F. Deng, Z. Chen, A control method for voltage balancing in modular multilevel converters, IEEE Trans. Power Electron. (2014), https://doi.org/10.1109/TPEL.2013.2251426.
[31] M. Zhang, L. Huang, W. Yao, Z. Lu, Circulating harmonic current elimination of a CPS-PWM-based modular multilevel converter with a plug-in repetitive controller, IEEE Trans. Power Electron. (2014), https://doi.org/10.1109/TPEL.2013.2269140.
[32] M. Moranchel, E. Bueno, I. Sanz, F.J. Rodríguez, New approaches to circulating current controllers for modular multilevel converters, Energies (2017) 10, https://doi.org/10.3390/en10010086.
[33] A.B. Rey-Boué, F. Martinez-Rodrigo, N.F. Guerrero-Rodríguez, L.C. Herrero-de Lucas, S. de Pablo, Enhanced controller for grid-connected modular multilevel converters in distorted utility grids, Electr. Power Syst. Res. (2018), https://doi.org/10.1016/j.epsr.2018.06.011.
[34] J. Peralta, H. Saad, S. Dennetière, J. Mahseredjian, S. Nguefeu, Detailed and averaged models for a 401-level MMC-HVDC system, IEEE Trans. Power Deliv. 27 (2012) 1501–1508, https://doi.org/10.1109/TPWRD.2012.2188911.